Reflection-Transmission of Nonlinear Waves in Channel Bends.

C.B. Harbitz

Department of Mathematics, Mechanics Division,
University of Oslo,
P.O.Box 1053 Blindern, 0316 OSLO 3, Norway

April 8, 1992

Abstract

A finite difference model based on the Boussinesq equations is applied to investigate nonlinear reflection-transmission of energy for solitons in L-shaped and T-shaped channel bend configurations. The reflection and transmission coefficients for the incident waves are discussed in terms of the ratios of the channel widths, and the ratio between the width of the deflected channel and the length of the incident wave. Nonlinearity and dispersion are found to be of minor importance within the investigated range of amplitudes and wavelengths.

1 Introduction

Large water waves associated with seismic activity, landslides or avalanches have in several cases caused serious destructions and loss of lives. The destructions are significantly aggravated when the waves occur in narrow fjords. Several times three or more successive waves have been reported for such events. Harbitz et al. (1992) linked this phenomenon to standing waves caused by trapping of wave energy in certain fjord geometries. For further insight into trapping effects, a systematic analysis of wave reflection and transmission in idealized fjord geometries is desirable. The aim of this paper is to analyse the reflection and transmission properties of single wave pulses associated with deflection or dividing of narrow channels. The analysis will also be relevant for evaluation of the sheltering capability of harbours and breakwaters.

Most previous analyses of reflection coefficients or diffraction patterns are made for wave trains incident to semi-infinite breakwaters or wave trains in channels of varying width or depth. Analytical solutions for reflection and diffraction of waves around the end of a semi-infinite breakwater are mainly based on mathematically analogous problems in diffraction of light by a semi-infinite screen (Sommerfeld, 1896). This approach was first applied by Penney and Price (1944, 1952), who extended the procedure by super position to the breakwater gap situation. They showed that the diffraction of waves through a single gap in a breakwater depends on whether the gap is small or not compared with the length of the incident waves. They assumed the height of the waves to be small compared with their length, but stated that the results will not be altered seriously if the waves are of moderate height.

Putnam and Arthur (1948) verified a modified version of the solutions by Penney and Price (1944) by comparison with results from a laboratory investigation. Pos (1985) simulated both numerically and experimentally symmetrical and asymmetrical gap wave diffraction with good correlation. He found secondary waves radiating from the tips of the breakwaters clearly evident in the experimental configuration, and concluded that these secondary waves is an important mechanism for wave energy transfer into the lee of

the breakwaters. Bettess et al. (1984) present numerical solutions for waves incident upon a semi-infinite breakwater and parabolic shoal, where both diffraction and refraction are present. Madsen and Warren (1984) verified a numerical dispersive long-wave model based on the Boussinesq equations against analytical as well as experimental results also for diffraction around breakwaters.

Dalrymple (1989) provides analytical expressions for the reflection coefficients associated with the channel transition, for linear waves propagating from a narrow rectangular channel into a wider rectangular channel. For this simple geometry the periodic wave field consists of the plane wave in each section plus progressive guided waves as well as evanescent standing waves at the discontinuity. He finds significant reflections due to resonance in the wider channel when the width of this channel corresponds to multiples of the wavelength. The reflection coefficient is a function of two parameters: the width of the wider channel relative to the wavelength, as well as the ratio of the channel widths.

2 Basic equations

In the present paper we are concerned with finite amplitude long waves in shallow water. These weakly dispersive waves are described by the Boussinesq equations, usually obtained by expansions in two small parameters, which are here named α and ε. The first parameter is a measure of nonlinearity, whereas the second is a measure of dispersion which is related to the deviations from hydrostatic pressure. Among several derivations of shallow water equations the works by Wu (1981) and Pedersen (1989) are particularly relevant in the present context.

Following Pedersen (1989), the equations are formulated in a Cartesian coordinate system with horizontal axes, ox^* and oy^*, in the undisturbed water level and the vertical axis, oz^*, pointing upwards. The asterisks indicate dimensional quantities. The fluid is confined to $-h^* < z^* < \eta^*$ and the depth averaged velocity potential is denoted by ϕ^*. A characteristic depth h_0, wavelength ℓ and amplitude αh_0 are introduced to form the dimensionless

variables

$$\begin{array}{llll} x^* = \ell x & y^* = \ell y & z^* = h_0 z & t^* = \ell(gh_0)^{-\frac{1}{2}} t \\ h^* = h_0 h & \eta^* = \alpha h_0 \eta & \phi^* = \alpha\ell(gh_0)^{\frac{1}{2}}\phi & e^* = \rho g \alpha^2 h_0^2 e \end{array} \tag{1}$$

where g is the acceleration of gravity, t^* is time, ρ is the density of the fluid and e^* is the mechanical energy per unit area in the fluid motion.

In the case of constant depth, $h \equiv 1$, the Boussinesq equations read:

$$\dot{\eta} + \nabla \cdot \{(1 + \alpha\eta)\nabla\phi\} = O(\alpha\varepsilon) \tag{2}$$

$$\dot{\phi} + \frac{1}{2}\alpha(\nabla\phi)^2 + \eta - \frac{1}{3}\varepsilon\nabla^2\dot{\phi} = O(\varepsilon^2, \alpha\varepsilon) \tag{3}$$

where $\dot{\eta}$ is defined as $\frac{\partial\eta}{\partial t}$, $\dot{\phi}$ as $\frac{\partial\phi}{\partial t}$, ∇ is the horizontal component of the gradient operator and $\varepsilon = (h_0/\ell)^2$, which is small according to the long wave assumption. By omitting terms of $O(\varepsilon, \alpha)$ in equations (2) and (3), we obtain the linear and hydrostatic shallow water equations. The set of equations (2) and (3) has an exact solution representing a solitary wave propagating with constant shape and speed. The solution may be implicitly expressed as an integral (Pedersen, 1988). To the leading order the solution becomes

$$\eta' = \frac{a}{\cosh^2[(\frac{3}{4}a)^{\frac{1}{2}}(x' - (1 + \frac{a}{2})t')]}(1 + O(\varepsilon, \alpha)) \tag{4}$$

where a is the maxcimum value of $\eta' = \eta^*/h_0$, $x' = x^*/h_0$ and $t' = (g/h_0)^{\frac{1}{2}}t^*$.

At a vertical and impermeable wall with unit normal vector $\vec{n}$ the zero flux boundary condition is expressed by

$$\frac{\partial\phi}{\partial n} \equiv \vec{n} \cdot \nabla\phi = O(\varepsilon^2, \alpha\varepsilon) \tag{5}$$

The wave energy per unit area is introduced for the analyses of energy reflection in sec.4, and is expressed by

$$e = \frac{1}{2}(\eta^2 + (1 + \alpha\eta)((\nabla\phi)^2 + \frac{1}{3}\varepsilon\dot{\eta}^2)) + O(\varepsilon^2, \alpha\varepsilon, \alpha^2) \tag{6}$$

Wave energy per unit area to lowest order is obtained by omitting terms of $O(\varepsilon, \alpha)$.

3 Finite difference representaion of the basic equations

The numerical approximation to a parameter f at a grid-point with coordinates $(\beta\Delta x,\ \gamma\Delta y,\ \kappa\Delta t)$ where Δx, Δy and Δt are the grid increments, is denoted by $f^{\kappa}_{\beta,\gamma}$. In order to make the difference equations more readable we introduce the symmetric difference operator, δ_x, by:

$$\delta_x f^{\kappa}_{\beta,\gamma} = \frac{1}{\Delta x}(f^{\kappa}_{\beta+\frac{1}{2},\gamma} - f^{\kappa}_{\beta-\frac{1}{2},\gamma}) \tag{7}$$

and the midpoint average operator, $^{-x}$, by:

$$(\overline{f}^{x})^{\kappa}_{\beta,\gamma} = \frac{1}{2}(f^{\kappa}_{\beta-\frac{1}{2},\gamma} + f^{\kappa}_{\beta+\frac{1}{2},\gamma}) \tag{8}$$

Difference and average operators with respect to the other coordinates y and t are defined correspondingly. We note that all combinations of these operators are commutative. To abbreviate the expressions further we also group terms of identical indices inside square brackets, leaving the super- and subscripts outside the bracket. These notations are adopted from Pedersen and Rygg (1987).

The equations (2) and (3) are discretized on a grid that is staggered in time only, calculating the quantities $\eta^{n}_{i,j}$, $\dot{\phi}^{n}_{i,j}$ and $\phi^{n+\frac{1}{2}}_{i,j}$. The difference equations read

$$[\delta_t\eta = -\delta_x\{(1+\alpha\overline{\eta}^{x,t})\delta_x\phi\} - \delta_y\{(1+\alpha\overline{\eta}^{y,t})\delta_y\phi\}]^{n-\frac{1}{2}}_{i,j} \tag{9}$$

$$[\dot{\phi} + T + \eta - \frac{\epsilon}{3}(\delta_x^2+\delta_y^2)\dot{\phi} = 0]^{n}_{i,j} \tag{10}$$

where

$$[T^n = \frac{1}{2}\alpha\{(\delta_x\overline{\phi}^{x})^{n-\frac{1}{2}}(\delta_x\overline{\phi}^{x})^{n+\frac{1}{2}} + (\delta_y\overline{\phi}^{y})^{n-\frac{1}{2}}(\delta_y\overline{\phi}^{y})^{n+\frac{1}{2}}\}]_{i,j} \tag{11}$$

Besides there is the kinematic relation

$$[\delta_t\phi = \dot{\phi}]^{n}_{i,j} \tag{12}$$

The solution procedure for equations (9) and (10) is explained at length in Pedersen(1988). Extensive testing concerning stability, convergence etc.

of the numerical model may be found in Pedersen and Rygg (1987). The stability criterion for the linearized difference scheme reads:

$$\Delta t^2 < \left(\frac{1}{\Delta x^2} + \frac{1}{\Delta y^2} \right)^{-1} + \frac{4}{3}\varepsilon \tag{13}$$

In the explicit solution method for the discrete version of the linear and hydrostatic shallow water equations, applied in sections 4.2.1 and 4.3.1, the time increment is chosen in accordance with the more restrictive standard Courant Friedrich Levy (CFL) criterion, which corresponds to eq.(13) with $\varepsilon \equiv 0$.

4 Results

4.1 Computational domain

We consider a channel domain with an L-bend or a T-bend configuration, fig.1. The T-bend is not necessarily symmetrical about the center line of section 2 of the channel, see fig.1b. The depth is constant, i.e. $h \equiv 1$, and the no flux boundary condition is applied along all sidewalls of the channel, except at the end, where the values of η and ϕ corresponding to a soliton input are specified, fig.1. The no flux condition is applied also along this end when the entire soliton with length λ has entered the computational domain. The halflength $\lambda/2 = \lambda^*/(2h_0)$ of the incident soliton is defined as the distance between the two points where the surface elevation is $a/2$, i.e. $\lambda/2 = 4\ln(\sqrt{2}+1)/\sqrt{3a}$.

The results will be presented in terms of the ratio of the channel widths, $\gamma = b_2/b_1$ and $\kappa = b_3/b_1$, fig.1, and the ratio between the width of channel section 2 and the halflength of the incident soliton, $\beta = 2b_2/\lambda$.

The integrated wave energy located in section 1 of the channel, fig.1, is denoted by E_1. The reflection in the bend is completed when E_1 attains the approximately constant value C_r, the energy reflection coefficient, after first being equal to one until the reflection starts, and then sometimes close to zero before the reflected wave has returned to section 1, cf. figs.3,4 and 10a.

For the T-bend configuration the integrated wave energy located in section 3 of the channel, fig.1b, is correspondingly denoted by E_3. The transmis-

sion in the bend is completed when E_3 attains the approximately constant value C_t, the energy transmission coefficient of section 3, after first being equal to zero until the transmission starts, cf. fig.10b.

4.2 Numerical experiments with L-bend configuration

4.2.1 Reflection-transmission of wave energy

To exclude effects of nonlinearity and dispersion, the reflection coefficient for the L-bend configuration is first calculated by the linear and hydrostatic shallow water equations. For constant depth, C_r is simply a function of the two non-dimensional parameters γ and β. Except for $\gamma = 0.2$, C_r increases monotonously with β for $\beta < 4.8$, fig.2, i.e. the reflection increases with decreasing wave length relative to the width of channel section 2. The curves for C_r vs. β might perhaps attain a maximum for all values of γ if the upper value of β is not limited to 4.8. Note that $C_r \to 0$ when $\beta \to 0$ for $\gamma = 1.0$. For the narrowest channel possible, the width of both channel sections is one grid distance. Provided that $\Delta x = \Delta y$, the numerical set of equations is then identical to the one-dimensional form also in the channel bend (cf. Pedersen, 1986, 1989). Hence the total transmission can be deduced directly from the numerical scheme. The smooth curve for $\gamma = 1.0$, fig.2, gradually approaching zero for decreasing β, ensures that this is really a physical effect, not simply a numerical one. From fig.2 it seems like C_r attains its least value for $\gamma = 1.0$ when $\beta < 0.6$, and for some $\gamma > 1$ when $\beta > 0.6$. Single wave pulses originate no resonance effects causing extraordinary reflection, as was found by Dalrymple (1989) for a periodic wave propagating from a narrow rectangular channel into a wider rectangular channel.

4.2.2 Effects of dispersion and nonlinearity

By reducing the length, and thereby increasing the amplitude of the incident soliton, the combined effect of dispersion and nonlinearity becomes clear when comparing the results from the nonlinear Boussinesq equations with the results from the linear and hydrostatic shallow water equations. In figs.3a and 3b is compared the amount of reflected energy E_1 vs. t for

two choices of wavelengths and corresponding amplitudes, while γ and β are both unchanged. As expected the deviation between the results from the linear and hydrostatic shallow water equations and the nonlinear Boussinesq equations is more prominent for the shorter waves, fig.3b. Dispersive and nonlinear effects slightly reduce the amount of reflected energy E_1. Besides the curves resulting from the Boussinesq equations are somewhat accelerated, due to the increased phase speed of nonlinear waves. If both channel widths are doubled, i.e. β is doubled while γ, λ and a are all unchanged, there will be more time for dispersive effects to evolve the reflection, which will also increase the difference between the results of the linear and hydrostatic shallow water equations and the nonlinear Boussinesq equations, compare figs.3b and 4.

4.2.3 The influence of γ and β on the profile of the reflected wave

Profiles of the leftward propagating reflected wave seen from cross-sections along channel section 1, do not differ between the upper and the lower boundary if $\beta \ll 1$. However, when β increases, the difference becomes significant. The difference occurs closer to the front of the leftward propagating reflected wave the smaller the value of γ, fig.5.

Narrow channel section 2 ($\gamma < 1$), and long incident wave ($\beta \ll 1$): When both $\gamma < 1$ and $\beta \ll 1$, (e.g. by reducing the value of b_2, while keeping b_1 and λ constant), the reflected wave has got an approximate sech^2-shape all across section 1, fig.6a. However, by comparison with the incident soliton, fig.6b, it appears that the height of the reflected wave from fig.6a, is reduced without any corresponding change in wavelength. Thus the reflected wave, as opposed to a soliton, will slowly disintegrate due to nonlinear and dispersive effects. (In fig.6b, the surface elevation of the reflected wave has been displaced and scaled, such that its maximum is situated in $x = 0$, and matches the crest of the incident soliton).

Wide channel section 1 ($\gamma \ll 1$), and short incident wave ($\beta \not\ll 1$): When $\gamma \ll 1$ and $\beta \not\ll 1$, (e.g. by increasing the value of b_1, while keeping b_2

and λ constant), the sech^2-shape is better preserved for a wave profile along the upper boundary, but the wave profile then differs across section 1, fig.5a.

Wide channel section 2 ($\gamma \not\ll 1$ and/or $\beta \not\ll 1$):
If not both $\gamma \ll 1$ and $\beta \ll 1$, there is a negative surface displacement in the foremost part of the reflected wave, at least along the lower boundary, figs.5b,7. This depression is more prominent for larger values of γ. The spatial extension of the depression increases with β, fig.7b. When $\gamma = 2.0$ and $\beta \ll 1$, the reflected wave appears as a single, negative displacement, fig.7a. The mirror image of this wave about the x-axis (displaced and scaled as in fig.6b), compared with the incident soliton, again depicts a surface elevation which has about the same length, but a reduced height compared with the incident soliton, fig.8.

The preceding effects of varying γ and β are mainly qualitative results. As for the energy reflection, nonlinearity and dispersion causes that nor the exact wave pattern is uniquely determined by γ and β.

4.3 Numerical experiments with T-bend configuration

4.3.1 Reflection-transmission of wave energy

The reflection and transmission coefficients are again first calculated by the linear and hydrostatic shallow water equations. For the T-bend configuration, the coefficients are functions of the non-dimensional parameter κ, in addition to γ and β. Fig.9 depicts the values of C_r (the energy reflection coefficient) and C_t (the energy transmission coefficient of section 3) as functions of β for $\gamma = 0.2,\ 1.0,\ 2.0$ and $\kappa = 0.5,\ 1.0,\ 1.5,\ 2.0$. When $\kappa \geq 1$ the reflection coefficient C_r increases with κ and γ, and decreases with increasing values of β, as opposed to the L-bend configuration where C_r increases with β. This can be explained by the increasing value of C_t with β, which means that the wave energy is more easily transmitted to channel section 3 for the shorter wave lengths. Thus the behavior of C_t for the T-bend configuration is closely related to the behavior of C_r for the L-bend configuration with varying values of β .

For $\kappa = 0.5$, the preceding observations is not valid for $\gamma \leq 1$, fig.9. With $\gamma < \kappa = 0.5$ or $b_2 < b_3 = 0.5b_1$, the region connecting sections 1 and 2 reminds of the L-bend situation, which explains why C_r increases while C_t decreases with β for $\gamma = 0.2$.

The transmission of wave energy to channel section 2 depends on γ and β as for the L-bend configuration, i.e. the wave energy is more easily transformed to section 2 for the longer wave lengths.

For the T-bend configuration the reflection coefficient is not zero for the narrowest channel possible. With $\gamma = \kappa = 1.0$, $\beta = 0.033$, we find $C_r = 0.11$, while the remaining wave energy is equally distributed to channel sections 2 and 3. When $\gamma = 2.0$, $\kappa = 1.0$ and $\beta \to 0$, we find approximately that one quarter of the energy in the incident wave is reflected, one quarter is transmitted to section 3, while one half is transmitted to section 2 of double width. Correspondingly, when $\gamma = 1.0$, $\kappa = 2.0$ and $\beta \to 0$, approximately one quarter of the wave energy is reflected, one quarter is transmitted to section 2, while one half is transmitted to section 3.

Dispersive and nonlinear effects do not have any influence upon the amount of reflected energy E_1 within the investigated range of amplitude and wave lengths. The transmitted energy E_3 is slightly increased by these effects for $\beta = 0.6$, not influenced for $\beta = 1.2$ and slightly decreased for $\beta = 2.0$.

4.3.2 The wave pattern in the T-bend

For the T-bend configuration with $\gamma < 1 - \kappa$, (i.e. $b_2 < b_1 - b_3$), the profile of the reflected wave depends on β as for the L-bend configuration. Else the reflected wave is a negative displacement. The spatial extension of the depression increases with β.

The waves transmitted to sections 2 and 3 are always positive displacements. The wave heights increase in both sections with decreasing values of γ and κ. In section 2 the wave height decreases with increasing values of β.

A typical wave pattern after completion of the reflection-transmission in the T-bend configuration is depicted in fig.11a. Behind the primary wave in section 2, there is an oscillating wave train. Such a wave train also occurs in

the extended L-bend configuration, fig.12a, and is therefore not conditioned by a narrow width of section 2. On the other hand, a narrow width causes significant variation of the wave height perpendicular to the walls of section 2. This implies crosswise standing waves in this region. Comparisons with the corresponding results of the linear and hydrostatic shallow water equations, figs.11b and 12b, reveal that the oscillating wave train is clearly fortified by nonlinear effects.

5 Conclusions

A numerical model based on the Boussinesq equations is applied to investigate nonlinear reflection-transmission of wave energy for solitons in L-shaped and T-shaped channel bend configurations. The L-bend constitutes an incoming channel section where the incident soliton is specified, and a deflected channel section. The T-bend holds an additional section located as a straight continuation of the incoming one. The reflection and transmission coefficients for the incident waves are discussed in terms of the ratios of the channel widths, and the ratio between the width of the deflected channel and the length of the incident wave.

In the L-bend configuration, the amount of reflected energy increases when the length of the incident wave decreases relative to the width of the deflected channel, with an exception for the narrowest deflected channels. In other words the wave energy is more easily transmitted to the deflected channel for the longer wave lengths. This may partly explain why the longer longitudinal waves more easily escapes through certain fjord bend geometries, while shorter crosswise waves are trapped (cf. Harbitz et al., 1992). Total transmission is obtained in the L-bend when the wavelength approaches infinity and the channel sections has got the same width.

In the T-bend configuration, the preceding dependence of wavelength on the amount of reflected energy is valid as long as the width of the deflected channel is less than the difference between the widths of the incoming channel and the straight continuing channel. On the other hand, if the straight continuing channel is wider than the incoming channel, the reflection coefficient increases when the width of the deflected channel or the straight continuing

channel increases relative to the width of the incoming channel. The reflection coefficient increases when the length of the incoming wave increases relative to the width of the deflected channel. This means that the wave energy is more easily transmitted to the straight continuing channel for the shorter wave lengths, while the transmission to the deflected channel increases with the wave length, as for the L-bend configuration. Altogether the energy of the longer waves are easily transmitted to the deflected channel, while the energy of the shorter waves are reflected in the L-bend configuration and transmitted to the straight continuing channel in the T-bend configuration.

If the incident wave is long relative to the width of the deflected channel, while the incoming channel constitutes the widest part and the deflected channel constitutes the narrowest part of the channel system, the reflected wave is exclusively a positive surface displacement. Otherwise there is a negative surface displacement at least in the foremost part of the reflected wave. The spatial extension of the depression increases when the width of the deflected channel increases relative to the wavelength.

Within the investigated range of amplitudes and wavelengths, nonlinearity and dispersion are found to be of minor importance for the reflection-transmission of wave energy in channel bends. However, the exact wave pattern is influenced by these effects. In the L-bend configuration, dispersive effects are slightly increasing with decreasing length of the incident wave.

References

Bettess,P., Liang,S.C. and Bettess,J.A. 1984: Diffracton of Waves by Semi-Infinite Breakwater Using Finite and Infinite Elements. *International Journal for Numerical Methods in Fluids* vol. 4, 813-832.

Dalrymple,R.A. 1989: Water Waves past Abrupt Channel Transitions. *Applied Ocean Research* 1989 Vol. **11-4.**

Madsen,P.A. and Warren,I.R. 1984: Performance of a Numerical Short-Wave Model. *Coastal Engineering* **8** (1984), 73-93.

Harbitz,C., Pedersen,G. and Gjevik,B. 1992: Numerical Simulations of Large

Water Waves Due to Landslides. *Research Report in Mechanics, Dep. of Mathematics, University of Oslo* **92-1**.

Pedersen,G. 1986: On the Effects of Irregular Boundaries in Finite Difference Models. *International Journal for Numerical Methods in Fluids* vol. **6**, 497-505.

Pedersen,G. and Rygg,O.B. 1987: Numerical Solution of the Three Dimensional Boussinesq Equations for Dispersive Surface Waves. *University of Oslo, Research Report in Mechanics* **88-1**.

Pedersen,G. 1988: Three-Dimensional Wave Patterns Generated by Moving Disturbances at Transcritical Speeds. *Journal of Fluid Mechanics* Vol. **196**, 39-63.

Pedersen,G. 1989: On the Numerical Solution of the Boussinesq Equations. *Preprint Series, Dep. of Mathematics, University of Oslo* No. **1**.

Penney,F.R.S. and Price,A.T. 1944: Diffraction of Sea Waves by Breakwaters. *Directorate of Miscellanous Weapons Development Technical History* No. **26**, - Artificial Harbors, Sec. 3D, 1944.

Penney,F.R.S. and Price,A.T. 1952: The Diffraction Theory of Sea Waves and the Shelter Afforded by Breakwaters. *Philosophical Transactions of the Royal Society of London* A **244**, 236-253.

Putnam,J.A. and Arthur,R.S. 1948: Diffraction of Water Waves by Breakwaters. *Transactions, American Geophysical Union* Vol. **29**, No. **4**.

Pos,J.D. 1985: Asymmetrical Breakwater Gap Wave Diffraction Using Finite and IOnfinite Elements. *Coastal Engineering* **9** (1985), 101-123.

Sommerfeld, A. 1896: Mathematische Theorie der Diffraktion. *Math. Ann.* **47**, 317-324.

Wu,T.Y. 1981: Long Waves in Ocean and Coastal Waters. *Proc. ASCE, J. Eng. Mech. Div.* **107**, EM3, 501-522.

Figure captions

Figure 1:
a: L-bend configuration, b: T-bend configuration (asymmetrical). Dotted lines define limitations of channel sections 1-3 of widths b_1, b_2 and b_3 respectively, incident solitons specified at A-A.

Figure 2:
Reflection coefficient C_r vs. β, calculated by the linear and hydrostatic shallow water equations, for the L-bend configuration with $\gamma = 0.2,\ 0.5,\ 1.0,\ 1.5,\ 2.0$.

Figure 3:
Fraction of integrated wave energy in channel section 1, E_1 (scaled by integrated wave energy in total computational domain), vs. time for the L-bend configuration with $\gamma = 1.0$, $\beta = 2.4$, a: $a = 0.018$, $\lambda/2 = 15.0$, b: $a = 0.167$, $\lambda/2 = 5.0$.

Figure 4:
Fraction of integrated wave energy in channel section 1, E_1 (scaled by integrated wave energy in total computational domain), vs. time for the L-bend configuration with $\gamma = 1.0$, $\beta = 4.8$, $a = 0.167$, $\lambda/2 = 5.0$.

Figure 5:
Cross-section of leftward propagating reflected wave along upper (solid line) and lower (dotted line) boundary of channel section 1 for the L-bend configuration with $\beta = 1.2$, $a = 0.018$, $\lambda/2 = 15.0$, a: $\gamma = 0.2$, b: $\gamma = 2.0$.

Figure 6:
a: Cross-section of leftward propagating reflected wave along upper (solid line) and lower (dotted line) boundary of channel section 1 for the L-bend configuration with $\gamma = 0.2$, $\beta = 0.067$, $a = 0.018$, $\lambda/2 = 15.0$. b: Displaced and scaled version of dotted line from fig.a compared with incident soliton.

Figure 7:
Cross-section of leftward propagating reflected wave along lower boundary of channel section 1 for the L-bend configuration with $a = 0.018$, $\lambda/2 = 15.0$, a: $\beta = 0.067$, $\gamma = 0.2,\ 1.0,\ 2.0$, b: $\gamma = 0.2$, $\beta = 0.067,\ 1.0,\ 2.0$.

Figure 8:
Displaced and scaled version of mirror-image of long-dotted line ($\gamma = 2.0$) from fig.7a compared with incident soliton.

Figure 9:
Reflection coefficients C_r and transmission coefficients C_t vs. β, calculated by the linear and hydrostatic shallow water equations, for the T-bend configuration with $\gamma = 0.2,\ 1.0,\ 2.0$ and with $\kappa = 0.5,\ 1.0,\ 1.5,\ 2.0$.

Figure 10:
Fraction of integrated wave energy vs. time for the T-bend configuration with $\gamma = 1.0$, $\beta = 1.2$, $\kappa = 1.0$, $a = 0.167$, $\lambda/2 = 5.0$, a: channel section 1, E_1 (scaled by integrated wave energy in total computational domain) vs. time, b: channel section 3, E_3 (scaled by integrated wave energy in total computational domain) vs. time.

Figure 11:
Perspective view of surface displacement for the T-bend configuration. Paramater values as in fig.10, vertical exaggeration 75:1, a: calculated by the nonlinear Bousinesq equations, $(g/h_0)^{\frac{1}{2}}t^* = 70.0$, b: calculated by the linear and hydrostatic shallow water equations, $(g/h_0)^{\frac{1}{2}}t^* = 74.2$.

Figure 12:
Perspective view of surface displacement for extended L-bend configuration with $\gamma = 6.9$, $\beta = 8.3$, $a = 0.167$, $\lambda/2 = 5.0$, vertical exaggeration 75:1, a: calculated by the nonlinear Bousinesq equations, $(g/h_0)^{\frac{1}{2}}t^* = 70.0$, b: calculated by the linear and hydrostatic shallow water equations, $(g/h_0)^{\frac{1}{2}}t^* = 74.2$.

Figures

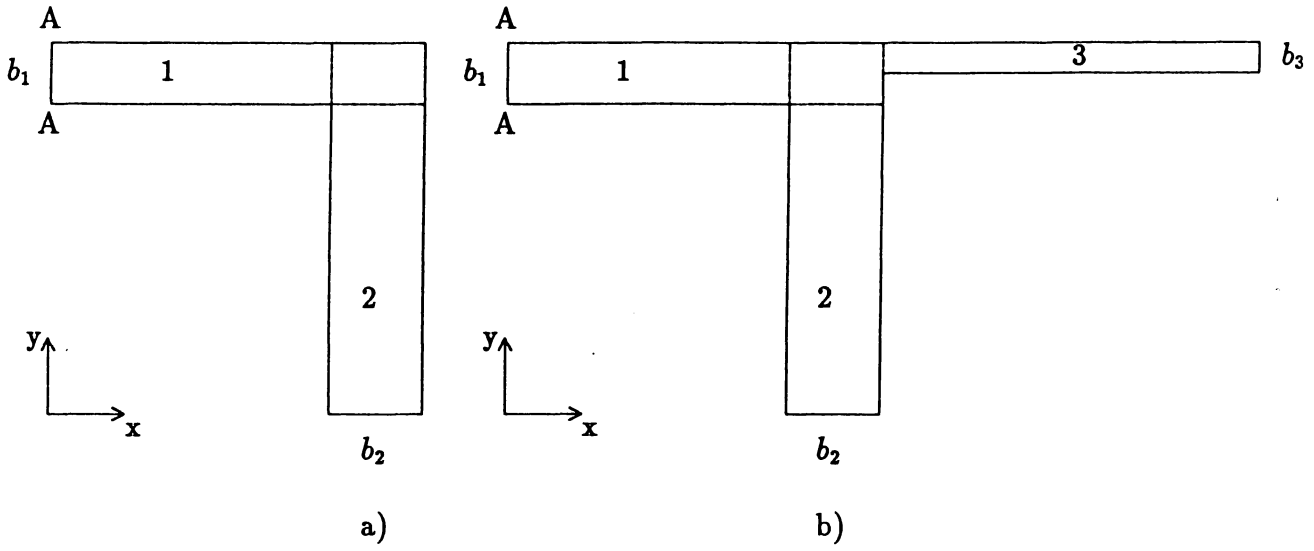

Figure 1:

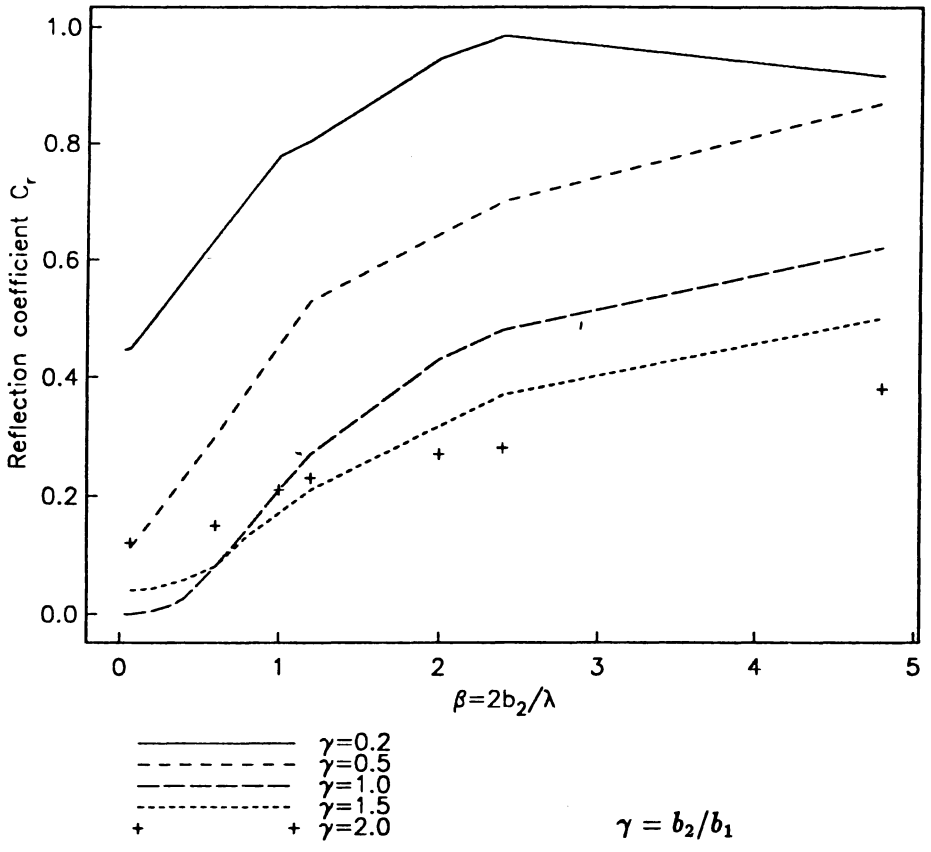

Figure 2:

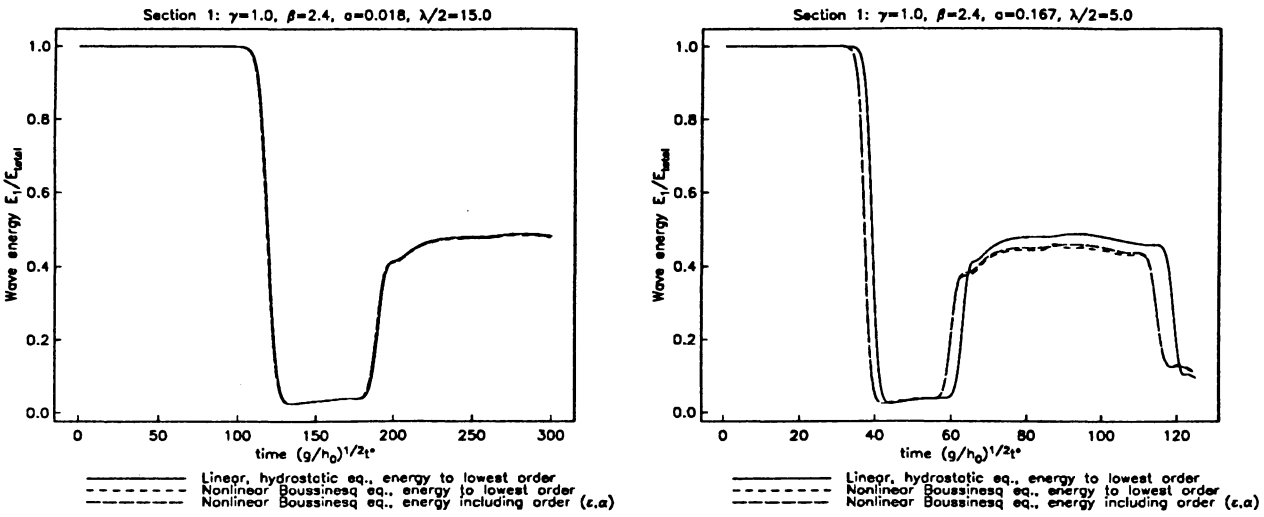

a) b)

Figure 3:

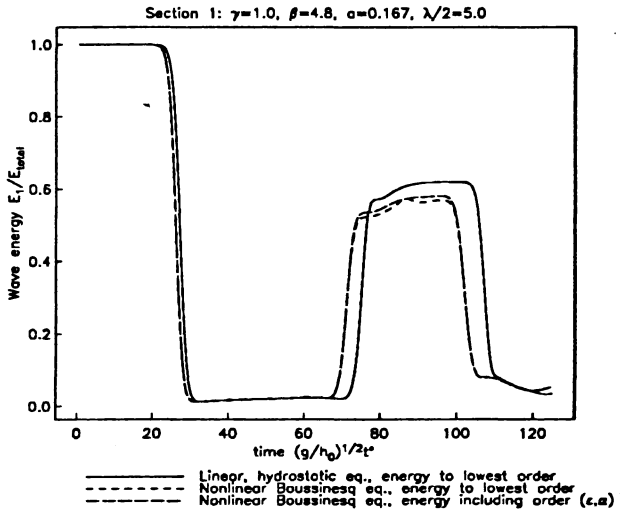

Figure 4:

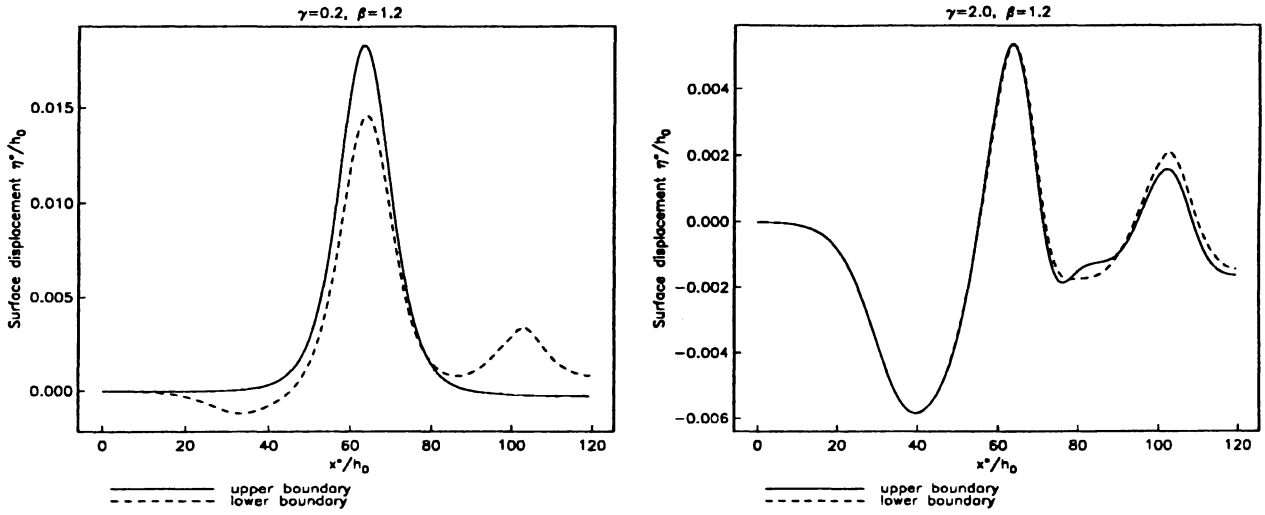

a) b)

Figure 5:

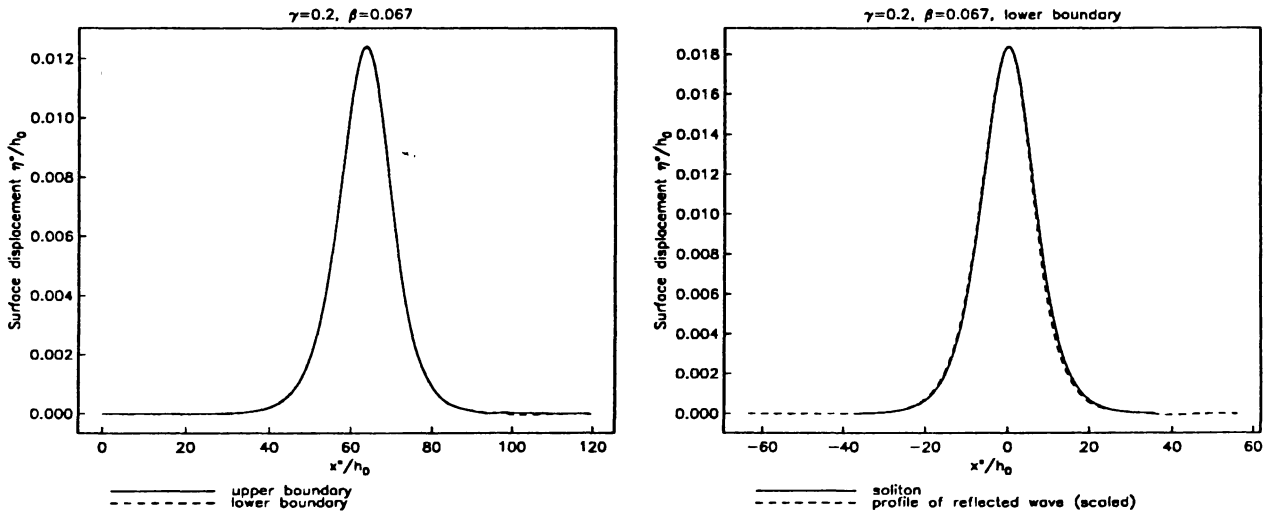

a) b)

Figure 6:

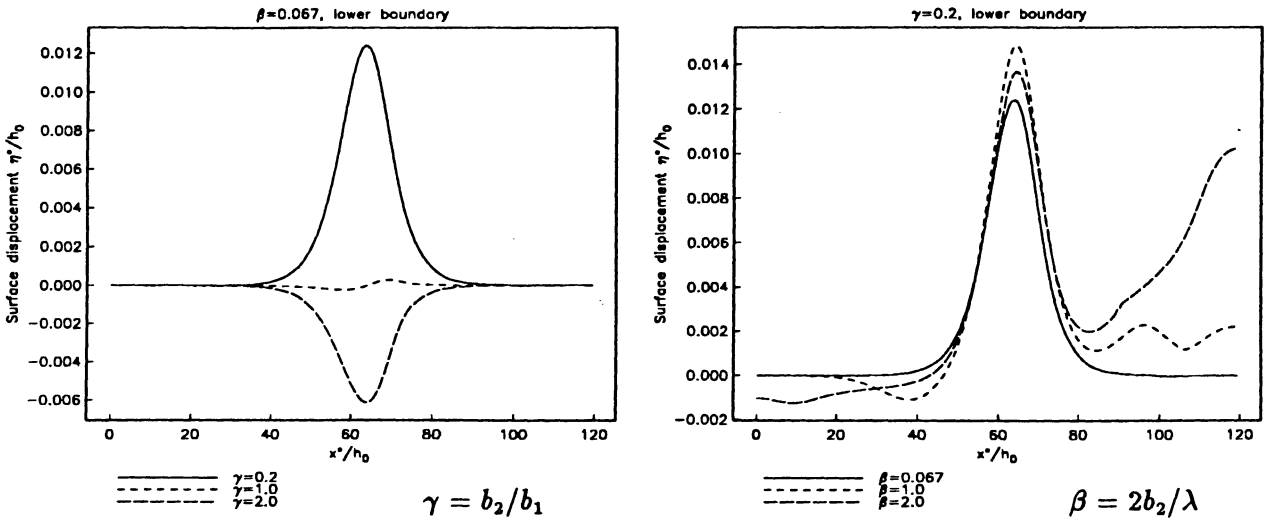

a) b)

Figure 7:

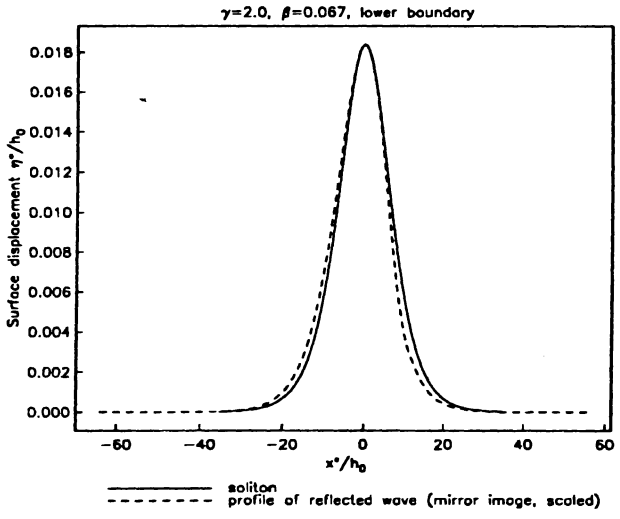

Figure 8:

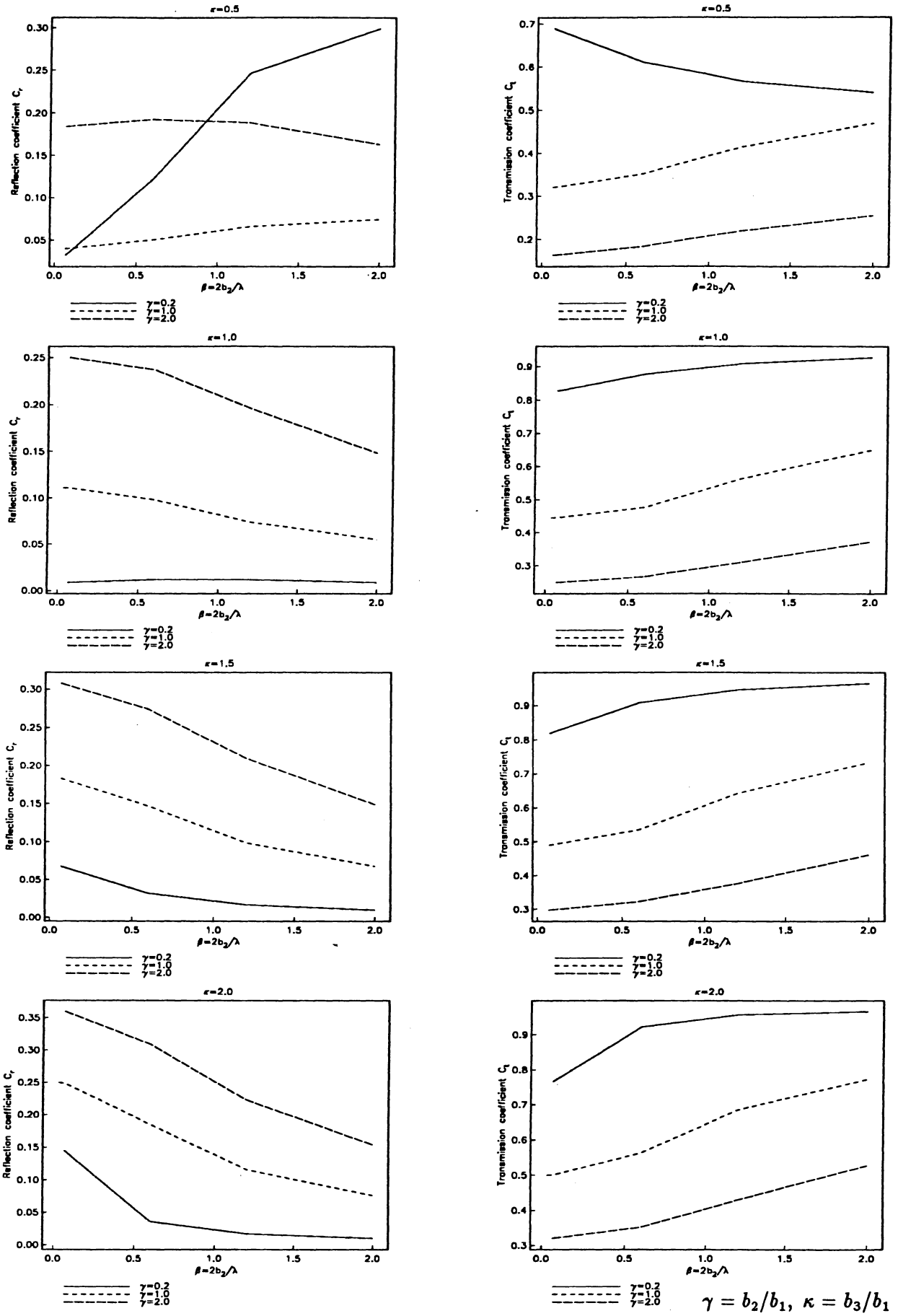
κ=0.5
Reflection coefficient C_r
Transmission coefficient C_t
$\beta=2b_2/\lambda$
γ=0.2
γ=1.0
γ=2.0
κ=1.0
κ=1.5
κ=2.0
$\gamma = b_2/b_1,\ \kappa = b_3/b_1$

Figure 9:

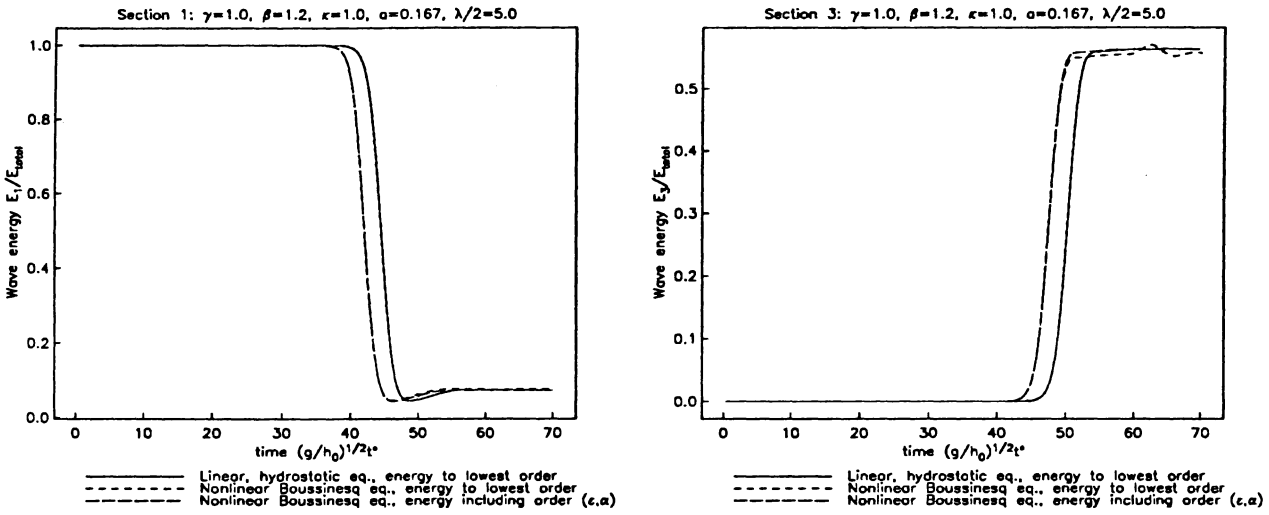
Section 1: γ=1.0, β=1.2, ε=1.0, α=0.167, λ/2=5.0
Wave energy E_1/E_{total}
time $(g/h_0)^{1/2}t^*$
Linear, hydrostatic eq., energy to lowest order
Nonlinear Boussinesq eq., energy to lowest order
Nonlinear Boussinesq eq., energy including order (ε,α)
Section 3: γ=1.0, β=1.2, ε=1.0, α=0.167, λ/2=5.0
Wave energy E_3/E_{total}
time $(g/h_0)^{1/2}t^*$
Linear, hydrostatic eq., energy to lowest order
Nonlinear Boussinesq eq., energy to lowest order
Nonlinear Boussinesq eq., energy including order (ε,α)

a) b)

Figure 10:

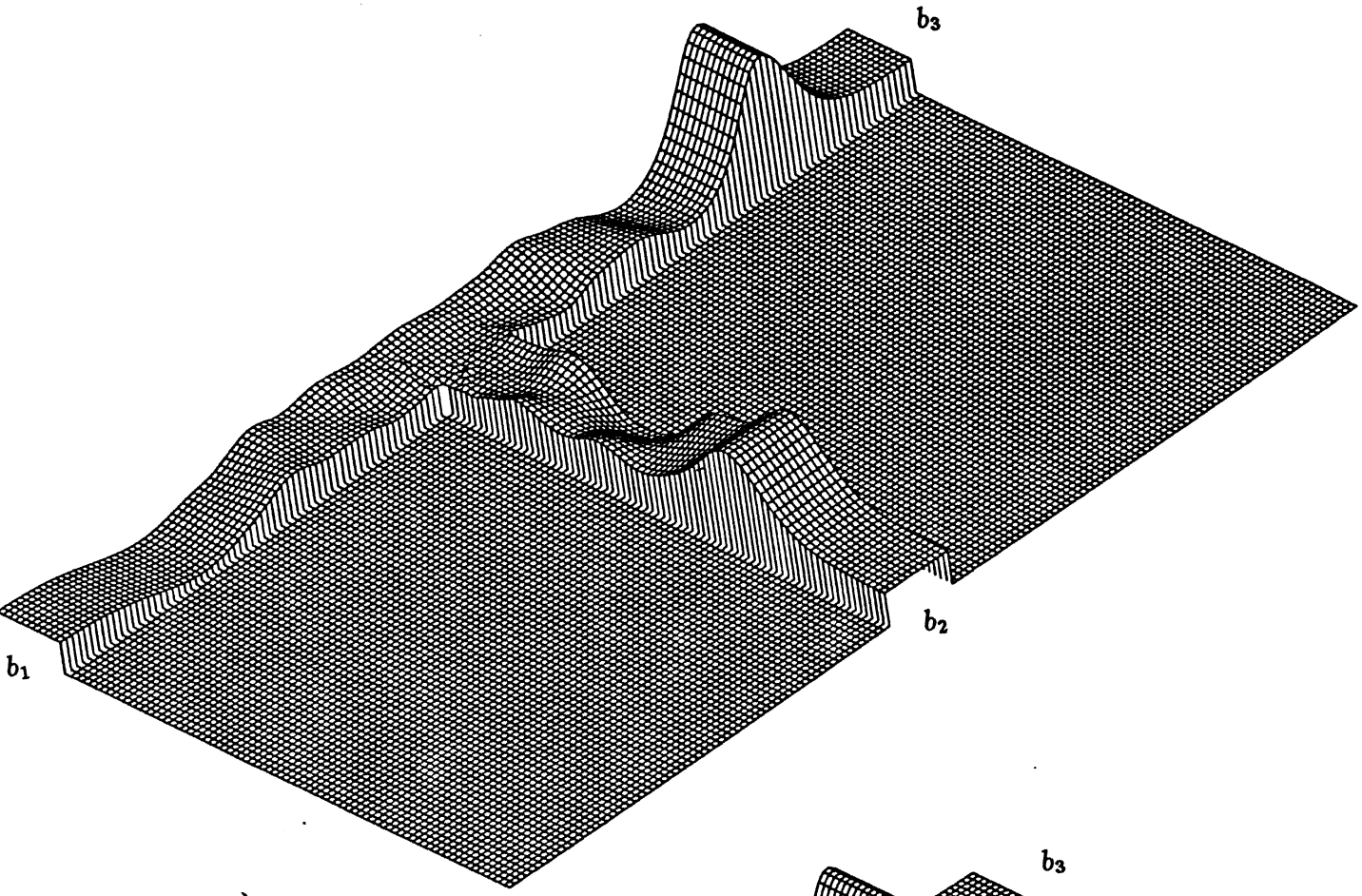

a)

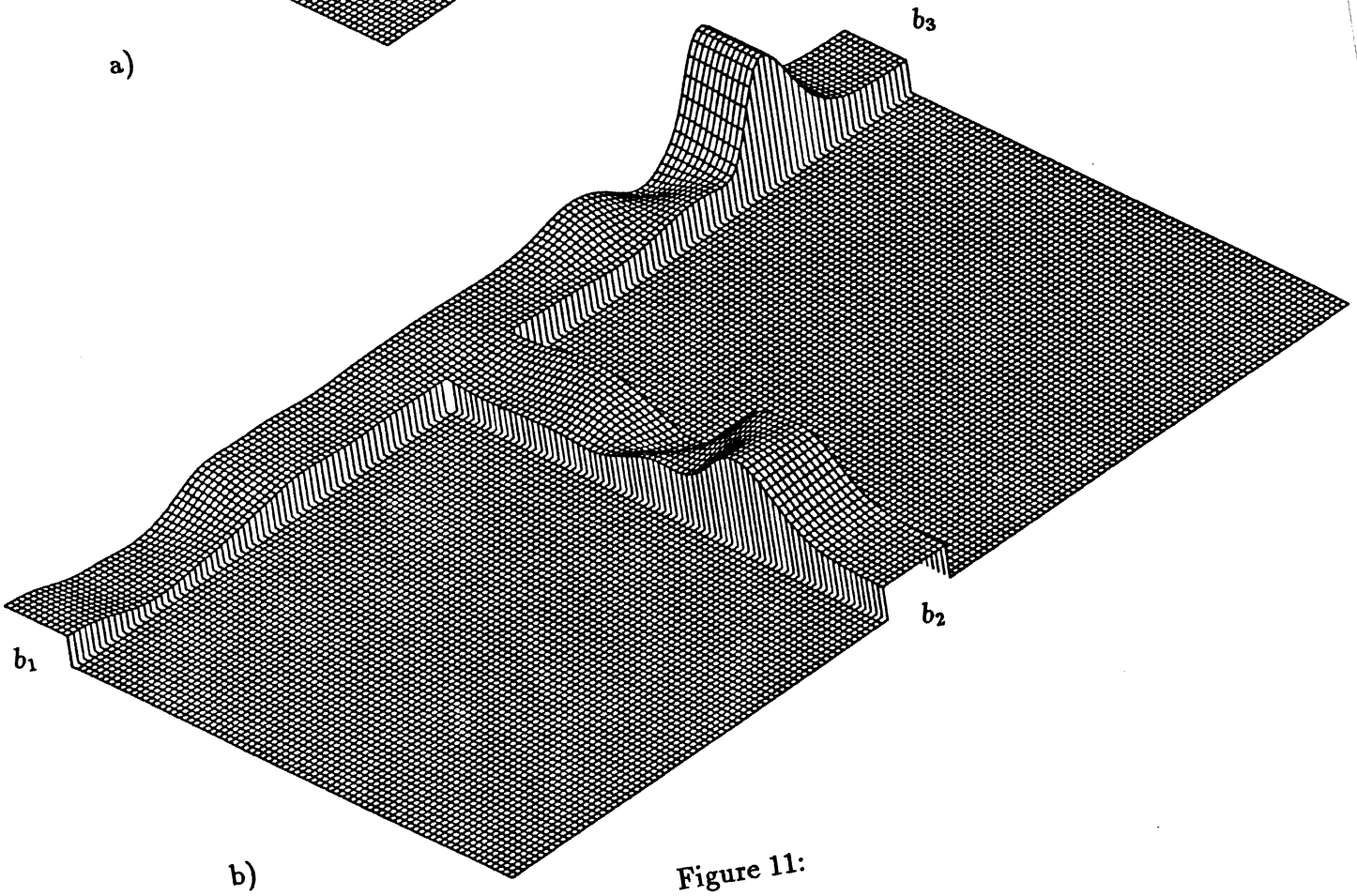

b)

Figure 11:

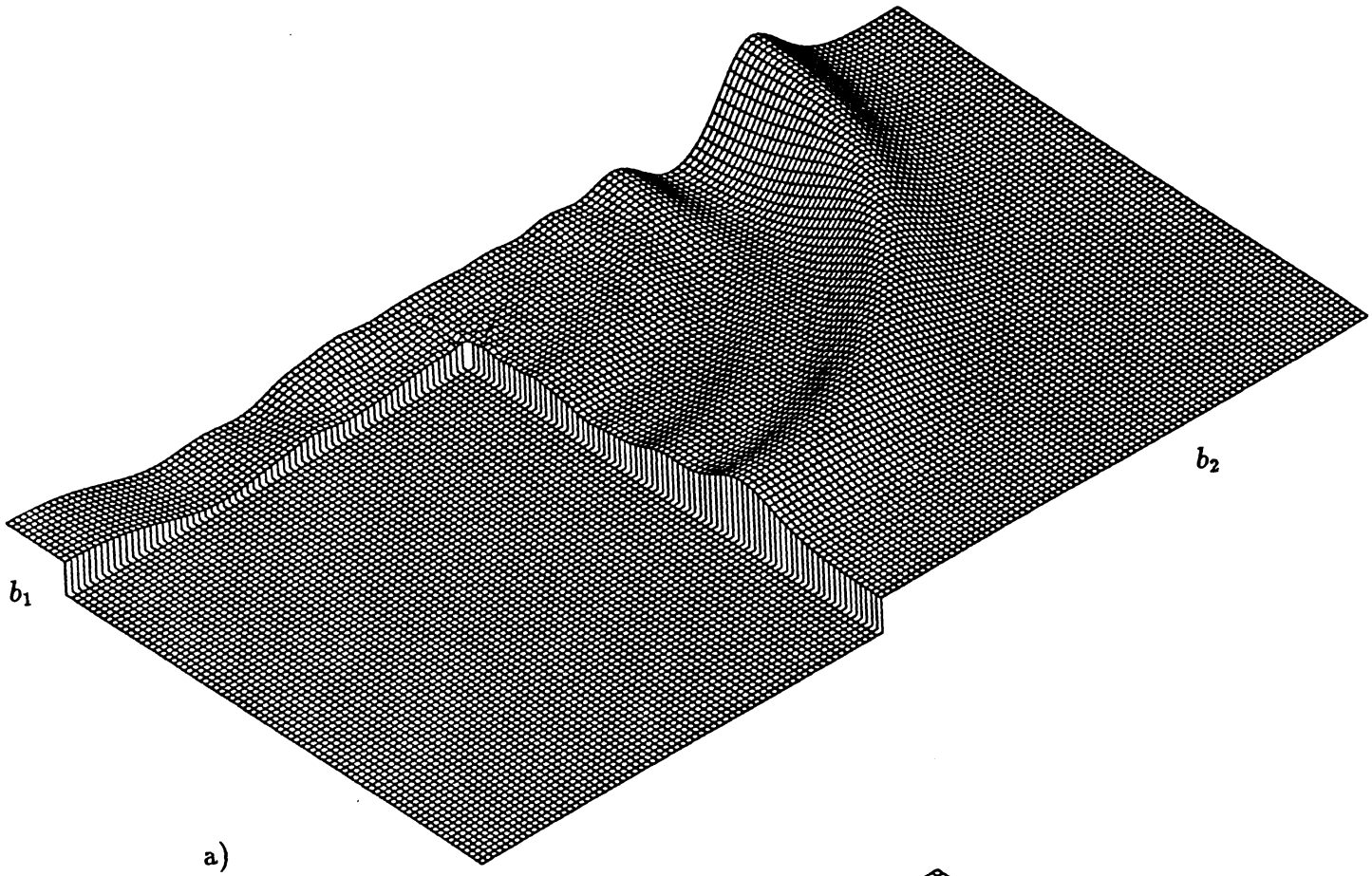

a)

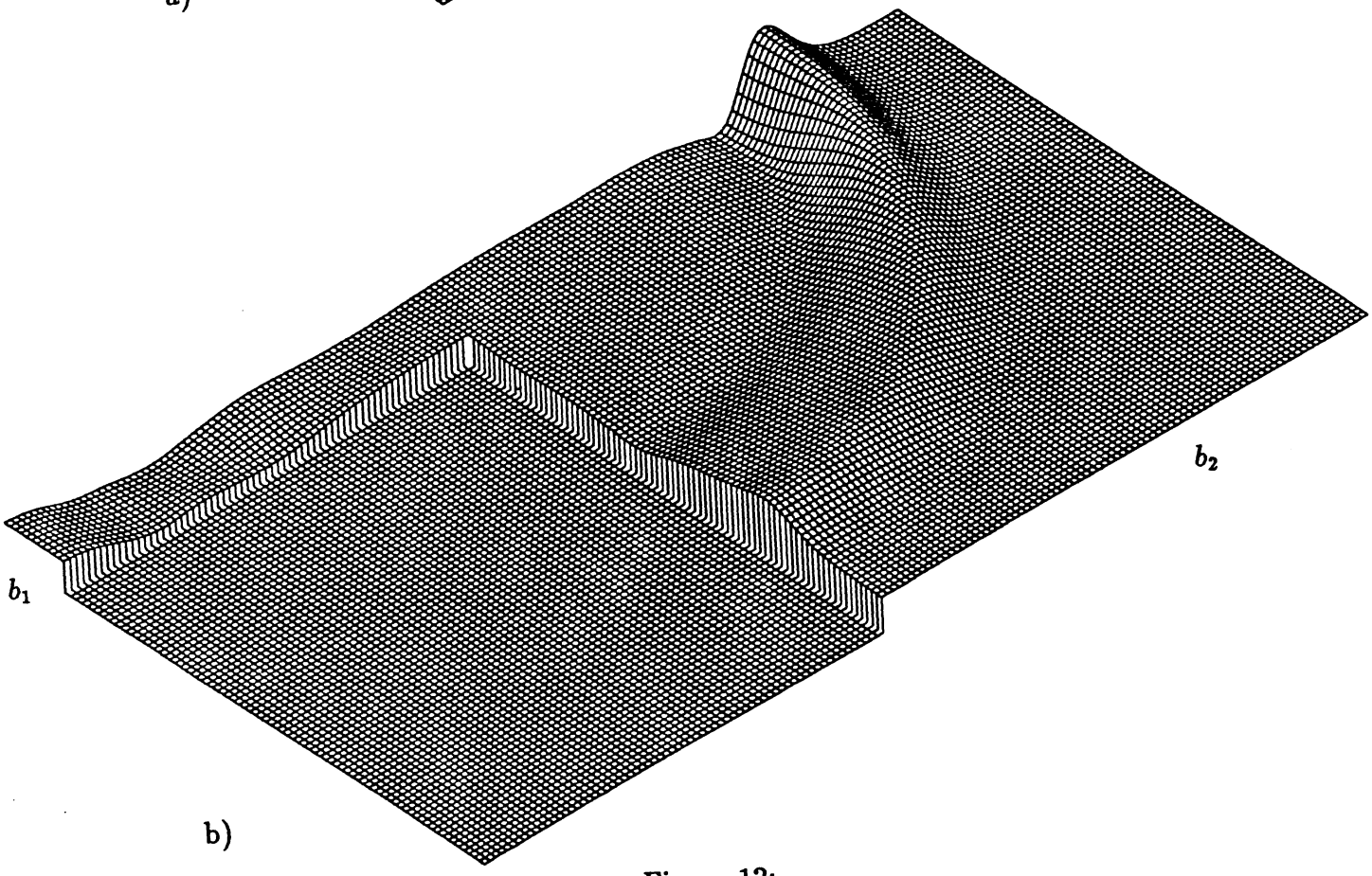

b)

Figure 12: